Supporting Information

Enhancing Electro-reduction of Nitrite to Ammonia by Loading Co_3O_4 on CuO to Construct Electrocatalytic Dual-site

Yan Zhou, Yunlong Meng, Xingzhao Wang, Jiabing Luo, Hanhan Xia, Wenle Li and Jun Zhang

Materials and chemicals

Copper sulfate pentahydrate ($CuSO_4 \cdot 5H_2O$, AR, 99%) and potassium nitrite (KNO_2 AR, 97%) were purchased from Aladdin, cobalt sulfate heptahydrate ($CoSO_4 \cdot 7H_2O$, AR, 99.5%), polyethylene glycol (PEG 2000), aqueous ammonia (NH_4OH, AR, 25.0% ~ 28.0%), and potassium hydroxide (KOH, AR) were purchased from SCR, trisodium citrate dehydrate and salicylic acid were purchased from MACKLIN, sodium hydroxide (NaOH, AR, 96.0%) was purchased from Kermel. The electrochemical workstation was CHI660E.

Characterization

All electrochemical tests were carried out on a CHI660E workstation. UV-vis spectra were tested on a SHIMADZU UV-2600 spectrophotometer. X-ray powder diffraction (XRD) images were taken on a Philips X' Pert diffractometer with Cu Kα radiation (λ = 0.15418 nm). Scanning Electron Microscope (SEM) was done on a Hitachi S-4800 electron microscope. Transmission Electron Microscope (TEM), High-Resolution TEM (HRTEM) and Selected Area Electron Diffraction (SAED) images were obtained on JEM-2100 UHR with an acceleration voltage of 200 kV. High-angle annular dark field-scanning TEM (HAADF-STEM) and the corresponding elemental mapping images were acquired using a FEI Titan Cubed Themis G2 300 S/TEM with a probe corrector and a monochromator at 200 kV. X-ray Photoelectron Spectroscopy (XPS) were recorded on an ESCALAB 250 analyzer (Thermo, America) with aluminum Kα radiation. All the peaks were corrected so that C 1s peak lines at 284.8 eV.

Preparation of CuO

CuO was synthesized by simple precipitation method. First, 110 mL of 0.1 M $CuSO_4 \cdot 5H_2O$ and 0.075 g PEG2000 were added to a 250 mL round bottom flask and heat it at 80℃ in an oil bath under reflux. Then, the newly prepared 3.5 M ammonia solution was added dropwisely into the flask under strong stirring. After further heating for 4 hours, black precipitate and blue liquid phase were obtained. The solid part was collected by vacuum filtration, fully washed with deionized

water and ethanol, and dried in a vacuum drying oven at 60℃ for at least 4 hours to obtain black CuO powder.

Preparation of Co_3O_4@CuO

For the preparation of 30%Co_3O_4@CuO, 110 mL of 0.1 M $CuSO_4 \cdot 5H_2O$ and 0.075 g PEG2000 were added into a 250 mL round bottom flask and heated at 80 ℃ in an oil bath under reflux. Then, the newly prepared 3.5 M ammonia solution was dropwisely added into the flask under strong stirring. After heating for 4 hours, 15 mL 0.2 M $CoSO_4$ solution was added into the flask dropwise and continued heating for 0.5 h. The precipitate was collected by filtration, fully washed with deionized water and ethanol, and dried in a vacuum drying oven at 60℃ for at least 4 hours to get Co_3O_4@CuO powder. For the preparation of Co_3O_4@CuO in other Co feeding ratios, 5 mL, 10 mL, and 20 mL 0.2 M $CoSO_4$ solution were added for 10% Co_3O_4@CuO, 20% Co_3O_4@CuO, and 40% Co_3O_4@CuO.

Preparation of Co_3O_4

Firstly, in a 250 mL round bottom flask, 0.075 g PEG2000 was dissolved in 100 mL deionized water and then 15 mL 3.5 M aqueous ammonia was added. Then it was heated to 80 ℃ in an oil bath. Secondly, 15 mL 0.2 M $CoSO_4 \cdot 7H_2O$ was added. After continuing heating and stirring for 0.5 hours, the precipitation was collected by vacuum filtration, washed with deionized water and ethanol adequately, and dried in a vacuum drying oven at 60℃ for at least 4 hours to obtain the dry green $Co(OH)_2$ powder. Finally, the green $Co(OH)_2$ powder was heated at 350℃ for 2 h in a muffle furnace to get the dark green Co_3O_4.

Mechanical mixing of CuO and Co_3O_4

For mechanically mixed material, it was obtained by mixing CuO and Co_3O_4 in a mass ratio of 1:0.3 and grinded in a mortar until uniform.

Preparation of electrode

For the preparation of working electrodes, 1 mg of catalyst powder, 200 μL of ethanol, and 2 μL of 5w% Nafion solution were mixed in a 1.5 mL centrifuge tube, and sonicated until uniform. Then the slurry was coating on a square carbon fiber paper (CP) with 1 cm^2 surface area and dried slowly. The carbon fiber paper was pre-treated before use. It was firstly bathed in ethanol for 30 min to clean up organic containments. Then the CP was washed by 3 M HCl solution for 30 min to remove any metallic and other impurities. Then the CP was bathed in deionized water for 30 min. All the three above-mentioned bathing was accompanied by ultrasonic treatment. Finally, the CP was

oxidized for hydrophilic treatment by 450℃ heating for 2 hours in a muffle furnace with heating rate of 10℃ per minute.

Electrochemical characterizations

The electrochemical tests were carried out on a CHI660E electrochemical workstation using an H-type cell separated by Nafion 117 membrane. The reference electrode was Ag/AgCl standard electrode with saturated KCl and the counter electrode was a 2.25 cm^2 Pt foil. For a typical amperometric *i-t* test, 30 mL electrolyte was used for every 30 minutes test in 30 mL working cell with magnetic stirring. After the test, appropriate amount of the electrolyte was collected and then stored in an air-tight centrifuge tube for quantifying ammonia concentration. The test potential started from -0.971 V vs. Ag/AgCl, which was before the onset potential of nitrite reduction. A total of five potentials were selected in -0.1 V intervals. The -0.971 V vs. Ag/AgCl corresponds to 0 V vs. SHE after calibration of Ag/AgCl electrode. The conversion to standard potential accords to the follow formula:

$$E\ (vs.\ SHE) = E\ (vs.\ Ag/AgCl) + E_{Ag/AgCl} + 0.059 \times pH$$

Determination and quantification of ammonia

The amount of ammonia was determined and quantified through Berthelot Reaction. The electrolyte after electrochemical test was firstly diluted by a certain number of times. For large current, the solution was diluted by 200 times, and for current less than 10 mA, it was diluted by 10 times. As for the preparation of chromogenic agent, three stock solutions were prepared. Solution A was prepared by dissolving 2.88 g trisodium citrate dehydrate, 2.88 g salicylic acid, and 2.00 g NaOH in 50 mL deionized water. Solution B was obtained by dissolving 0.1 g sodium nitroprusside in 10 mL deionized water. Solution C was prepared by mixing 700 µL 7w% ~ 14w% NaClO solution with 20 mL deionized water. 2 mL solution A, 200 µL solution B, and 1 mL solution C with different concentrations of $NH_3 \cdot H_2O$ were mixed and the absorbance were measured using an UV-Vis spectroscopy at 655 nm wavelength. The calibration graph was then obtained by plotting absorbance against ammonia concentration. The concentration of ammonia obtained by electrolysis was measured using the calibration graph with appropriate dilutions.

Determination of nitrite concentration:

The concentration of nitrite was determined by UV-vis spectrum and Lambert-Beer law. The color reagent for nitrite consisted of 0.2 g N-(1-naphthyl) ethylenediamine dihydrochloride, 4 g sulfonamide and 10 ml phosphoric acid (85 wt.% in H_2O), which was diluted to 50 ml aqueous solution using a 50 mL volumetric flask. For the quantification of nitrite in 50 ppm nitrite-N solution, we took 10 µL of the sample solution into 5 mL of deionized water (diluted for 500 times), added 1 ml of 1 M HCl, and finally added 0.1 mL of color reagent for nitrite. The color development process was completed after 20 min of standing. For the kinetic evaluation, we used a low concentration of potassium nitrite solution (50 ppm nitrite-N, 0.1 M KOH) to make the variation of nitrite concentration more obvious.

Details and theoretical basis of rotating disc electrode

Now that the suitable potential (+0.2 V vs. Ag/AgCl) for the detection of intermediates using a Pt electrode has been determined, we would use a rotating ring-disk electrode for the detection of intermediates in the NIRA reaction. The test was performed in a five-necked bottle containing 0.1 M KOH and 0.1 M KNO_2 electrolytes. The catalytic materials were drop-coated on the disk electrode in the middle of the rotating ring-disk electrode, and the LSV tests were performed on the disk electrode. The outer disk electrode (Pt ring) set at +0.2 V vs. Ag/AgCl was used to detect the intermediate products. When reduction products other than NH_3 are produced on the middle disk electrode, which are stable for a short time and can diffuse to the outer Pt ring to be electro-oxidized, an oxidation current is generated on the Pt ring electrode. Therefore, we can analyze the intermediates produced during the NIRA reaction based on the oxidation current at the platinum ring electrode (if the dual-site catalysis is established). Corresponding to the two electrodes, the test result contains two parts, one is the LSV current curve of the disk electrode (Fig. 3c) and the other is the oxidation current on the ring electrode (Fig. 3d) when the disk electrode is tested for LSV.

For the ring current curve of CuO (Fig. 3d, blue curve), the ring current changes little when the disk electrode potential is above -1.0 V vs. Ag/AgCl, corresponding to the tiny NIRA reaction current at the disk electrode. When lower than -1.0 V vs. Ag/AgCl, the NIRA current (Fig. 3c, blue curve) increases as the potential decreases and the ring current starts to increase sharply, implying that lots of intermediates are produced. In contrast to CuO, the ring currents of Co_3O_4@CuO (Fig. 3d, orange curve) and the mechanical mixing material (Fig. 3d, red curve) are much smaller than that of CuO, implying that the intermediate products reaching the ring electrode are significantly reduced. This reduction can be explained in the way that the involvement of Co_3O_4 is able to reduce the intermediates more efficiently, thus cutting the quantity of intermediates reaching the ring electrode, and this why mechanical mixing Co_3O_4 with CuO could improve the performance of CuO in electrocatalytic NIRA reaction. In conclusion, in conjunction with the previous section, we have provided two key phenomena for the evidence of the dual-site catalytic pathway of Co_3O_4@CuO material in electrocatalytic NIRA reaction, (a) the mechanical mixing of Co_3O_4 with CuO can also enhance the catalytic effect of CuO on the electrocatalytic NIRA reaction (Fig. 3b), and (b) the similar ring currents (amounts of immediate products) of Co_3O_4@CuO and mechanical mixing material, both of which are much lower than that of CuO (Fig. 3d). These two phenomena, one for hypothesis and one for verification, are sufficient to preliminarily justify the dual-site catalytic pathway of Co_3O_4@CuO in electrocatalytic NIRA reaction.

The dual-site catalytic mechanism has been demonstrated above. However, there are still two possible pathways, pathway 1 and pathway 2, for dual-site catalysis as shown in the Scheme 2. We can try to analyze the most probable pathway based on the available data. If we follow pathway 1, the nitrite is first reduced on CuO to intermediate products, which are then reduced to ammonia on Co_3O_4, and we prefer this pathway. Pathway 2 is the opposite of pathway 1. We prefer pathway 1 for two reasons. For reason one, the LSV current of Co_3O_4 is much smaller than that of CuO, as shown in Fig. 3c, suggesting the low catalytic activity of Co_3O_4 in nitrite reduction and producing immediate products. And that

means, if it follows pathway 2, it would be too challenging for Co_3O_4 to provide sufficient immediate products to support the high activity of Co_3O_4@CuO. For the second reason, the change trend of the intermediate product of Co_3O_4@CuO should be similar to that of the first catalytic site (the production center of intermediate products). For Co_3O_4@CuO and the mechanical mixing material (Fig. 3d), their ring currents increase faster at about -1.1 V like CuO, and their change pattern is similar to that of CuO despite the values. As for Co_3O_4 (Fig. 3d), its ring current decreases after -1.1 V, and increase greatly at about -1.6 V (where HER occurred and many bubbles blocked the surface of disk electrode during test), but we cannot find any similar fluctuations in the ring current curves for Co_3O_4@CuO and the mechanical mixing material, indicating that Co_3O_4 is probably not the first catalytic site. So, in summary, it is CuO analyzed more like the first catalytic site rather than Co_3O_4. And the pathway 1 is more like a reliable dual-site catalytic pathway.

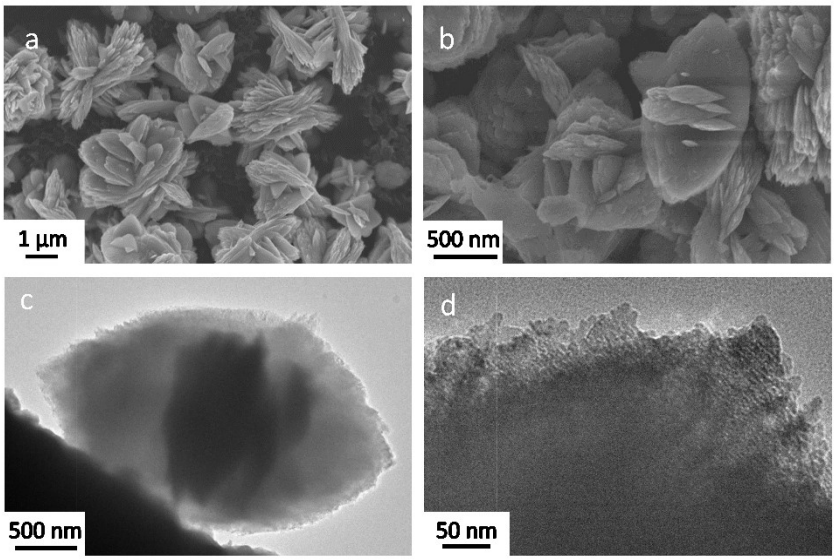

Fig. S1 (a, b) SEM images of CuO nano-followers; (c, d) TEM images of CuO.

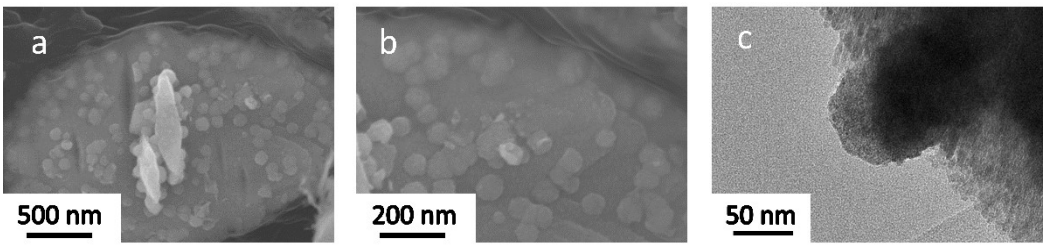

Fig. S2 (a, b) SEM images of Co_3O_4@CuO; (c) TEM images of Co_3O_4@CuO, the dark nanosphere is Co_3O_4.

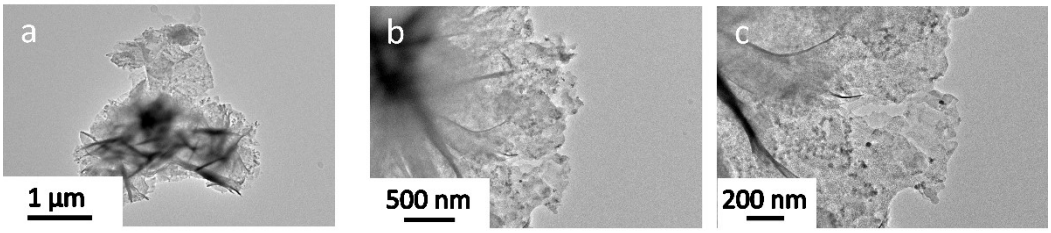

Fig. S3 TEM images of Co_3O_4 at different magnifications.

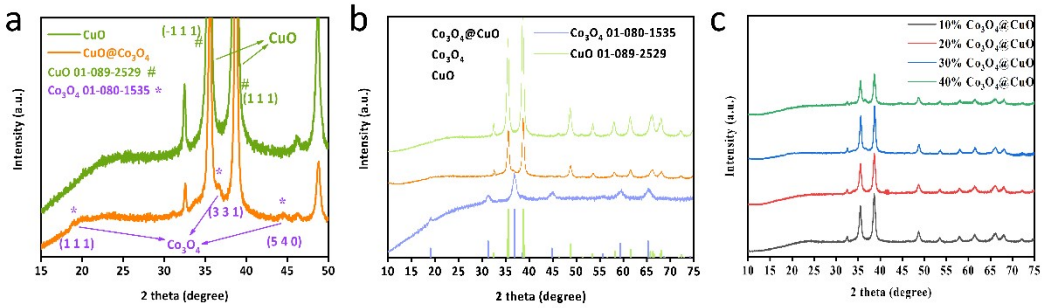

Fig. S4 XRD patterns of (a) Co_3O_4@CuO and CuO, (b) Co_3O_4@CuO, Co_3O_4 and CuO, (c) 10%Co_3O_4@CuO, 20%Co_3O_4@CuO, Co_3O_4@CuO, and 40%Co_3O_4@CuO.

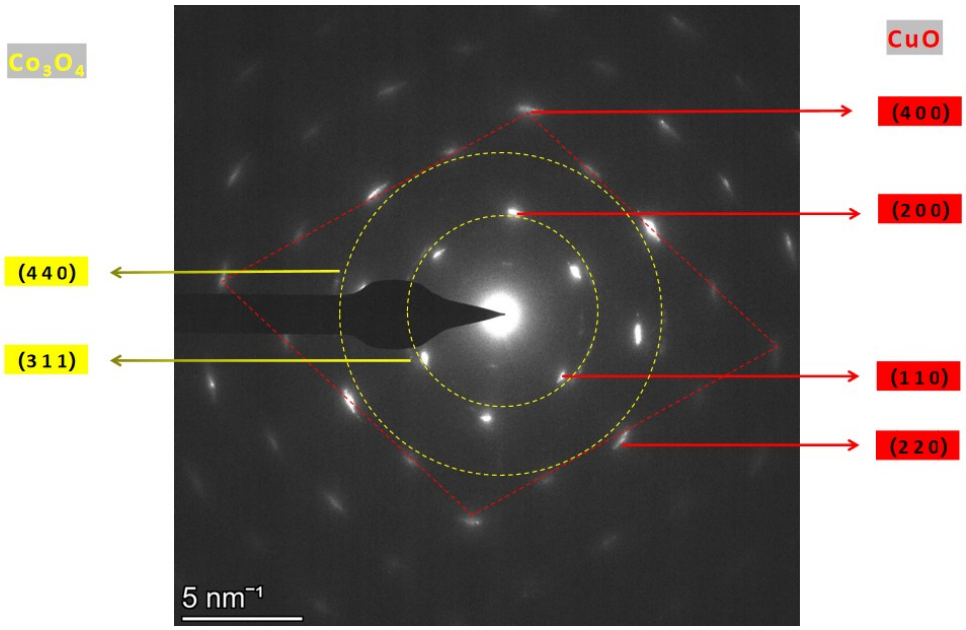

Fig. S5 SAED pattern of Co_3O_4@CuO nearby Co_3O_4 nanosphere.

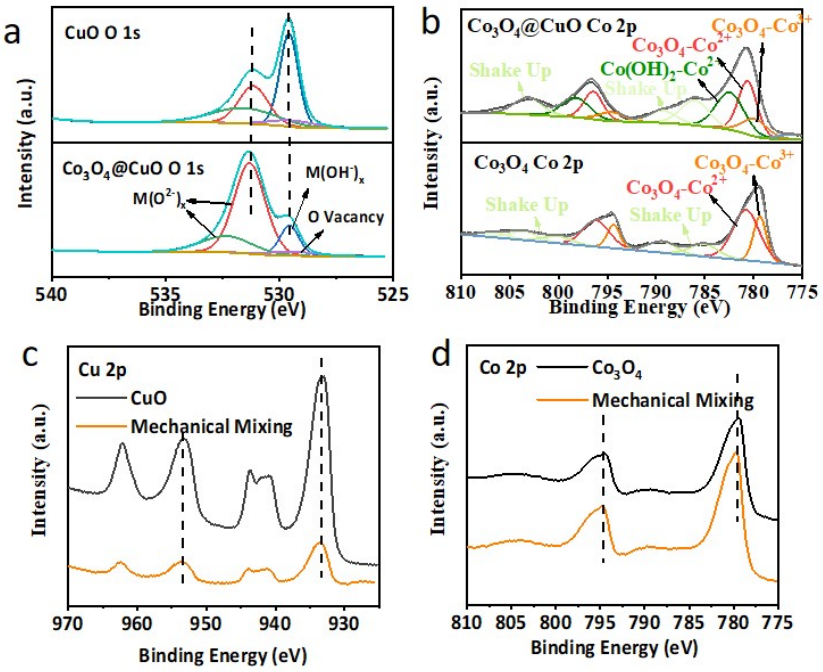

Fig. S6 XPS fine spectrum of (a) O 1s orbital for CuO and Co_3O_4@CuO, (b) Co 2p orbitals for Co_3O_4@CuO (up) and Co_3O_4 (bottom), (c) Cu 2p for CuO and mechanically mixed CuO and Co_3O_4, (d) Co 2p for Co_3O_4 and mechanically mixed CuO and Co_3O_4.

Fig. S7 Photos of Co_3O_4@CuO electrode surface at different potentials.

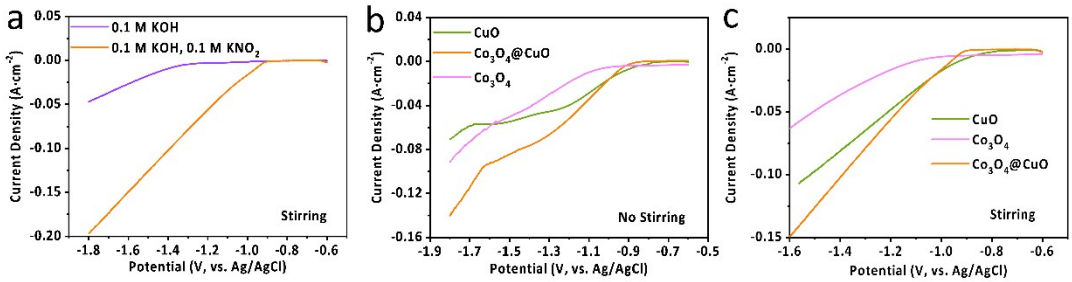

Fig. S8 (a) LSV curves comparation of Co_3O_4@CuO in 0.1 M KOH with or without 0.1 M KNO_2 under stirring condition. LSV curves of CuO and Co_3O_4@CuO in 0.1 M KOH and 0.1 M KNO_2 (b) without or (c) with stirring.

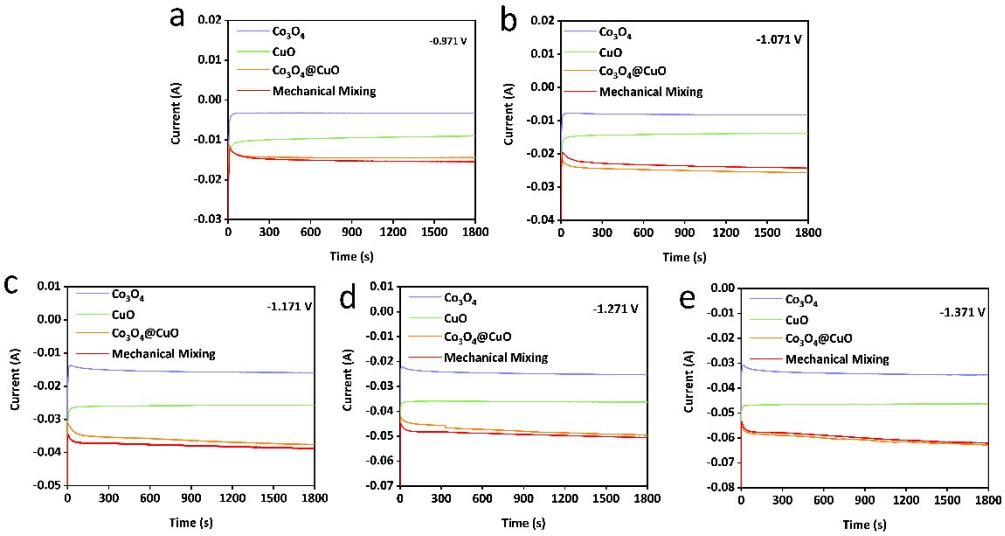

Fig. S9 Chronoamperometric curves for different cathode materials at different potentials vs. Ag/AgCl.

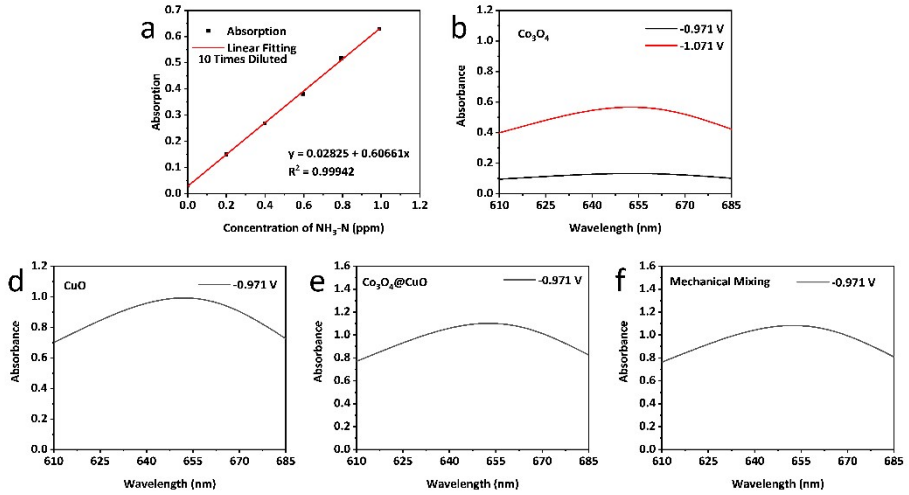

Fig. S10 (a) Standard ultraviolet light absorbance - NH_3-N concentration curves for 10 times diluted samples. (b-f) Ultraviolet light absorbance - wavelength curves in electrolyte with low NH_3 concentration.

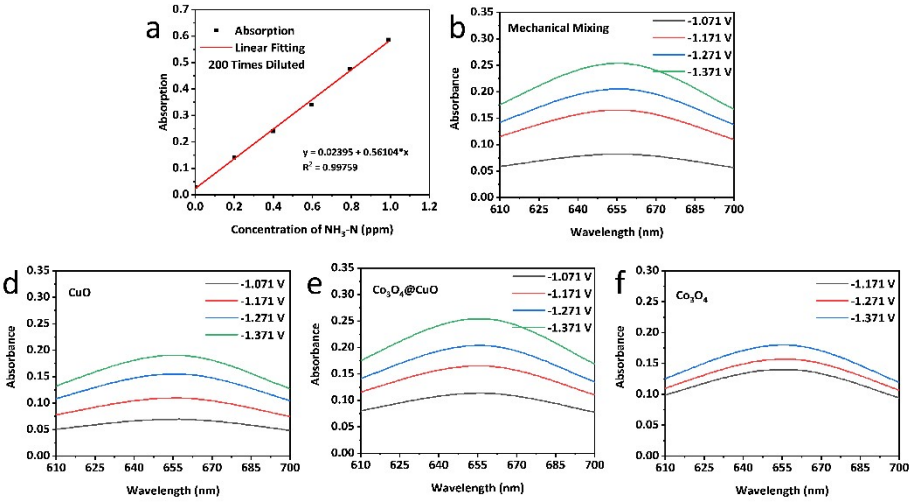

Fig. S11 (a) Standard ultraviolet light absorbance - NH_3-N concentration curves for 200 times diluted samples. (b - f) Ultraviolet light absorbance - wavelength curves for electrolyte samples of high NH_3 concentration.

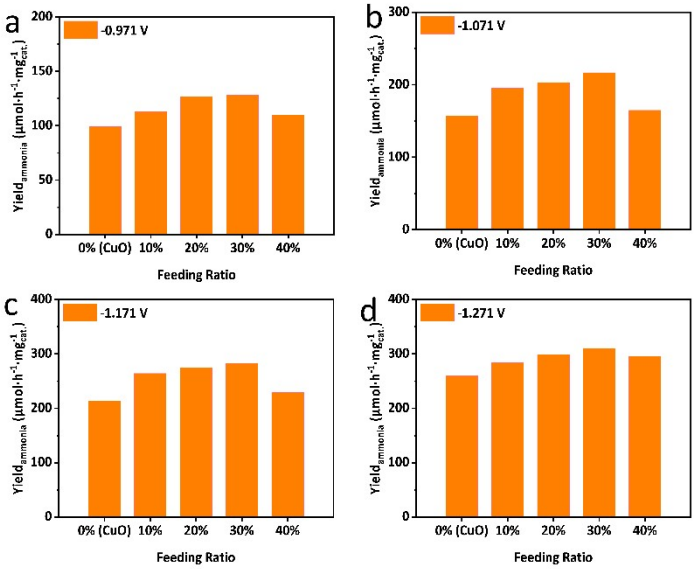

Fig. S12 Ammonia yield comparisons for cathode materials of different cobalt-copper feeding ratios under different potentials.

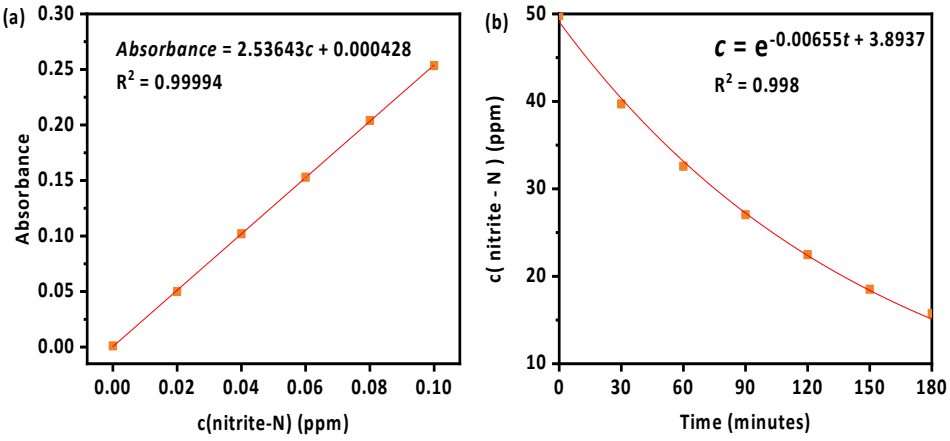

Fig. S13 (a) Standard fitting curve of UV-light absorbance against concentration of nitrite. (b) Curve of concentration of nitrite against time.

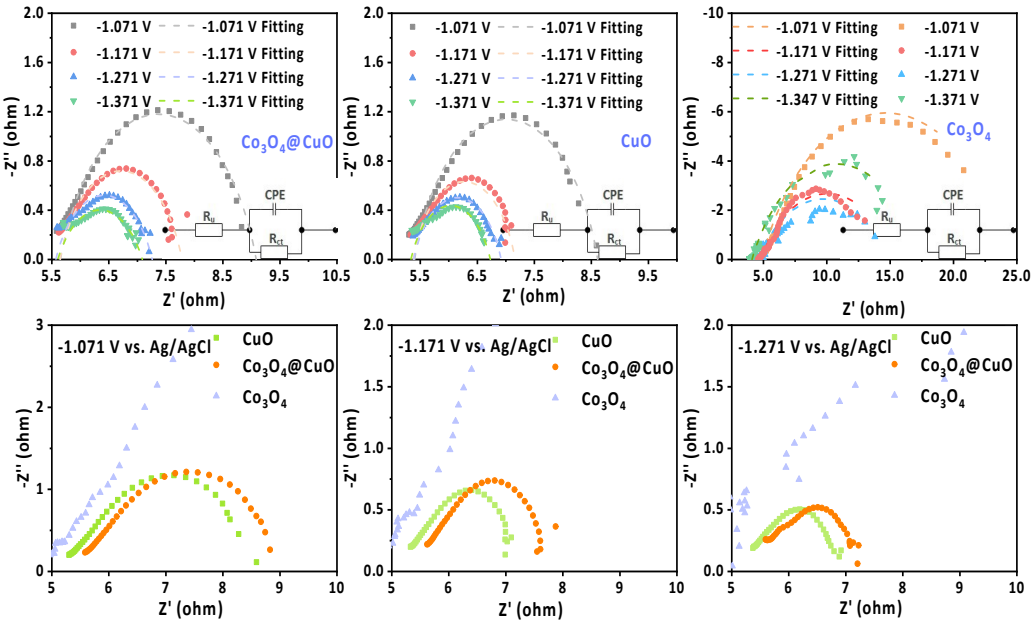

Fig. S14 EIS images for CuO, Co_3O_4@CuO and Co_3O_4 at different potentials vs. Ag/AgCl.

Table S1 Resultant R_{ct} after fitting EIS curves.

Potential (vs. Ag/AgCl) / Cathode Materials	-1.071	-1.171	-1.271	-1.371
CuO	3.2	1.8	1.5	1.4
Co_3O_4@CuO	3.4	2.1	1.7	1.5
Co_3O_4	19.6	10.66	10.34	13.3

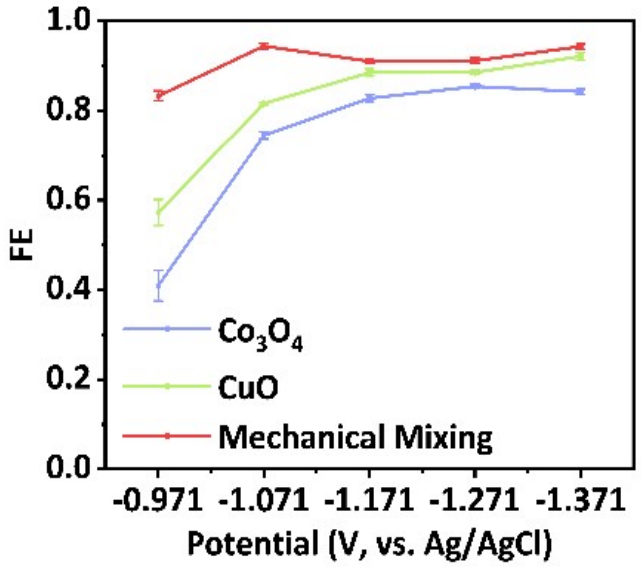

Fig. S15 Faradaic efficiency of different cathode materials

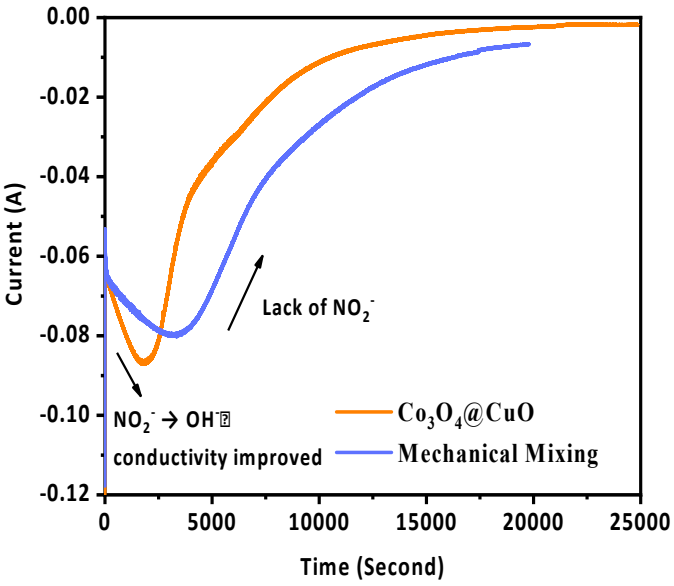

Fig. S16 Long-time *I-t* test at -1.3 V vs. Ag/AgCl of Co_3O_4@CuO and the mechanical mixing material (in 30 mL 0.1 M KOH and 0.1 M KNO_2 electrolyte).

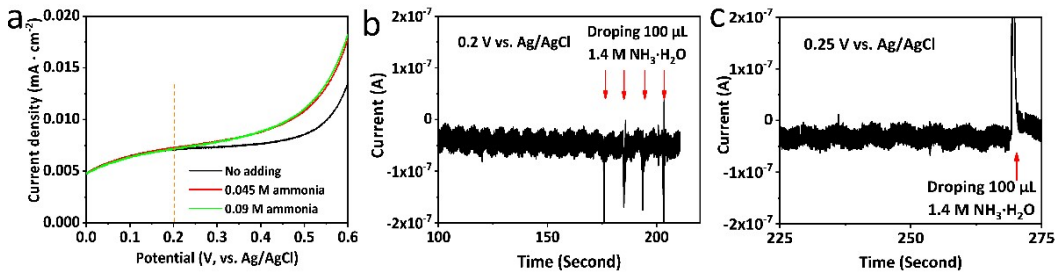

Fig. 17 (a) LSV curves of a Pt foil electrode in 30 mL 0.1 M KOH with 0.1 M KNO_2 before and after adding ammonia. (b) *I*-*t* curve of a Pt foil electrode in 30 mL 0.1 M KOH with 0.1 M KNO_2 electrolyte with adding ammonia at 0.2 V vs. Ag/AgCl. (c) *I*-t curve of a Pt foil electrode in 30 mL 0.1 M KOH with 0.1 M KNO_2 electrolyte with adding ammonia at 0.25 V vs. Ag/AgCl.